PHYSICAL REVIEW E **78**, 025301(R) (2008)

Dynamo action in Möbius flow

Anvar Shukurov,[1] Rodion Stepanov,[1,2] and Dmitry Sokoloff[3]
[1]*School of Mathematics and Statistics, Newcastle University, Newcastle upon Tyne, NE1 7RU, United Kingdom*
[2]*Institute of Continuous Media Mechanics, Academy of Sciences, 1 Korolyov Street, Perm, 614013, Russia*
[3]*Department of Physics, Moscow State University, Moscow, 119992, Russia*
(Received 3 March 2008; published 1 August 2008)

We demonstrate that flows of conducting fluid along a Möbius strip and related surfaces are hydromagnetic dynamos, i.e., they can produce an exponentially growing magnetic field from an infinitesimal seed. The critical magnetic Reynolds number in one of our models is as low as about 16. Together with other attractive features, this makes this flow an interesting candidate for a laboratory dynamo experiment.

DOI: 10.1103/PhysRevE.78.025301 PACS number(s): 47.65.−d, 52.30.Cv, 52.72.+v

Theory and applications of hydromagnetic dynamos have recently been invigorated by successful laboratory experiments that have confirmed the fundamental theory and revealed new prospects [1]. A necessary condition for dynamo action is that the induction time scale is shorter than the magnetic diffusion time scale, i.e., that the magnetic Reynolds number R_m exceeds a certain critical value R_m^* that depends on the flow geometry and boundary conditions,

$$R_\mathrm{m} = bV_0/\eta > R_\mathrm{m}^*, \tag{1}$$

where b and V_0 are the representative scale and speed of the flow, and η is the magnetic diffusivity. Among the smallest values known, $R_\mathrm{m}^* \approx 17$ is achieved for the Ponomarenko dynamo [2], implemented in the Riga dynamo experiment [3]. The values of R_m in liquid sodium experiments do not exceed about 100 [4]. It is therefore important to identify flows capable of dynamo action at modest values of R_m achievable in the laboratory.

We suggest that a flow of conducting fluid in a channel that envelopes the Möbius strip (or a similar surface) is a dynamo with a relatively low value of R_m^* suitable for a laboratory realization. A shell filled with rotating liquid sodium, as in the Perm dynamo experiment [4], can be suitable for such an experiment. The flow geometry in our case is rendered not by diverters or propellers, but by the shape of the channel. It is surprising that this idea has not been explored earlier. We note, however, a study of the electric current flowing along a Möbius strip [5].

A family of surfaces related to a Möbius strip has the following parametric representation in Cartesian coordinates:

$$x(u,v) = (R + v\cos nu)\cos u,$$

$$y(u,v) = (R + v\cos nu)\sin u, \tag{2}$$

$$z(u,v) = v\sin nu, \quad 0 \leqslant u < 2\pi, \quad |v| \leqslant a,$$

where R is the major radius of the strip, $a<R$ is its half width (the surface has self-intersections for $a>R$), and n is the number of full twists around the strip. A Möbius strip is obtained for $n=1/2$; single- and double-sided surfaces have odd and even values of $2n$, respectively. The variables u and v can be considered as curvilinear coordinates measured along and across the strip. As u increases, the surface is twisted clockwise for $n>0$ and anticlockwise for $n<0$.

We construct a related three-dimensional object, a Möbius channel with elliptical cross section shown in Fig. 1, via

$$x = [R + w(a\cos v\cos nu - b\sin v\sin nu)]\cos u,$$

$$y = [R + w(a\cos v\cos nu - b\sin v\sin nu)]\sin u, \tag{3}$$

$$z = -w(a\cos v\sin nu + b\sin v\cos nu),$$

where $0 \leqslant u < 2\pi$, $0 \leqslant v < 2\pi$, and $w < R/a$; a and b are the semimajor and semiminor axes of the ellipsoidal cross section, respectively ($a<R$ to avoid singularities). This surface is swept by an ellipse in the vertical plane rotating around its center while it moves around the z axis; R is the distance from the ellipse's center to the z axis; all the channels discussed below have $w=1$ at the surface. While making one rotation around the z axis, the ellipse makes n rotations around its center. The variables (w,v,u) represent right-handed, nonorthogonal, curvilinear coordinates, with u the azimuthal angle ($\tan u = y/x$), v the polar angle in the ellipse's plane, and w an analog of the dimensionless polar radius of the polar coordinates in the ellipse plane (Fig. 1). The (w,v) plane is orthogonal to the (x,y) plane.

A solenoidal flow tangent to the channel surface is introduced as

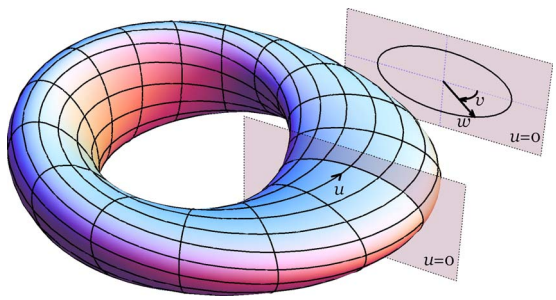

FIG. 1. (Color online) A Möbius channel ($n=1/2$) with elliptical cross section, as given by Eq. (3) with $R/b=4$, $a/b=2$. The coordinate lines of u and v are shown solid, the former being the streamlines. The inset shows the cross section, as indicated, with the definitions of v and w illustrated. The surface shown is $w=1$.

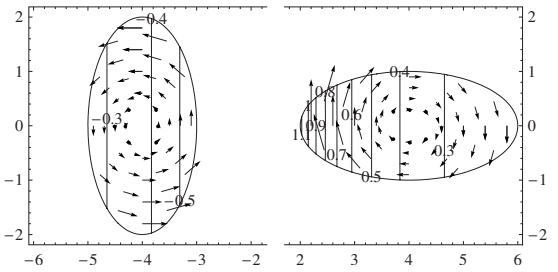

FIG. 2. Velocity field (4) with $V_0=1$ in the cross sections $u=0$ (right panel) and $u=\pi$ (left panel) (see Fig. 1): the meridional flow (V_x,V_z) is shown with vectors, and the angular velocity Ω_z, with labeled contours.

$$\mathbf{V}=\frac{V_0}{s}\frac{\partial \mathbf{r}}{\partial u},\quad V^i=\frac{\partial r^i}{\partial \xi^j}\tilde{V}^j, \tag{4}$$

with $r^i=(x,y,z)$ from Eq. (3), where $\tilde{V}^i=(0,0,V_0/s)$ are contravariant velocity components in the curvilinear coordinates $\xi^i=(w,v,u)$, V^i are those in Cartesian coordinates, $V_0=\text{const}$, and $s=R+w(a\cos v\cos nu-b\sin v\sin nu)$ is the distance to the axis $x=y=0$. We assume that the conductor is stationary ($\mathbf{V}=\mathbf{0}$) outside the channel. Flow in the channel of Fig. 1 has positive helicity, $\mathbf{V}\cdot\boldsymbol{\nabla}\times\mathbf{V}>0$. Velocity field (4) is solenoidal: $\boldsymbol{\nabla}\cdot\mathbf{V}=|g|^{-1/2}\partial_i(|g|^{1/2}\tilde{V}^i)$, where $g=\det(g_{ik})=(abws)^2$ with g_{ik} the metric tensor, hence $\boldsymbol{\nabla}\cdot\mathbf{V}=\partial_u(V_0abw)\equiv 0$. The normal velocity at the channel surface is zero because each streamline is a coordinate curve $w=\text{const}$, $v=\text{const}$ and the channel surface is a coordinate surface $w=\text{const}$. This flow, illustrated in Fig. 2, has constant azimuthal velocity, so $\Omega_z\propto s^{-1}$.

We solve the induction equation for the vector potential $\mathbf{A}$ of magnetic field $\mathbf{B}$,

$$\frac{\partial \mathbf{A}}{\partial t}=R_{\mathrm{m}}\mathbf{V}\times\mathbf{B}+\nabla^2\mathbf{A},\quad \mathbf{B}=\boldsymbol{\nabla}\times\mathbf{A}, \tag{5}$$

in a Cartesian box with fixed velocity (4) and $\eta=\text{const}$ throughout the domain, where the magnetic Reynolds number is defined with respect to the smaller dimension of the channel as in Eq. (1), and the time unit is b^2/η. We employ a gauge such that $\eta\boldsymbol{\nabla}\cdot\mathbf{A}=\Phi$, where Φ is the electric potential; with this gauge, $\boldsymbol{\nabla}\times(\eta\boldsymbol{\nabla}\times\mathbf{A})=-\eta\boldsymbol{\nabla}^2\mathbf{A}$ for $\eta=\text{const}$, so that Φ does not appear in Eq. (5). Although $\mathbf{V}$ is discontinuous at the channel surface, both $\mathbf{B}$ and $\mathbf{A}$ are continuous. Solutions relevant to the dynamo problem have $\mathbf{B}\to\mathbf{0}$ for $s^2+z^2\to\infty$; $|\mathbf{B}|$ grows for $R_{\mathrm{m}}>R_{\mathrm{m}}^*$. The velocity field is mapped from the (w,v,u) frame to the Cartesian frame using the inversion of Eq. (3):

$$u=\arctan y/x,\quad v=\arctan p/q,\quad w=\sqrt{q^2+p^2},$$

$$pb=(R-\sqrt{x^2+y^2})\sin nu-z\cos nu, \tag{6}$$

$$qa=(\sqrt{x^2+y^2}-R)\cos nu-z\sin nu.$$

The induction equation can be written componentwise in curvilinear coordinates (w,v,u) (we omit these equations here), where it becomes evident that equations for the corresponding magnetic field components B_w, B_v, and B_u are coupled via the diffusion term due to the curvature. This makes obvious the analogy with the Ponomarenko dynamo and makes it clear that the dynamo must be slow, i.e., the magnetic field growth rate of a given mode tends to zero as $R_{\mathrm{m}}\to\infty$ [8]. Another similar system is a helical pipe dynamo (see Ref. [6], and references therein).

We use the sixth-order Runge-Kutta adaptive time stepping and seventh-order centered finite differences in space,

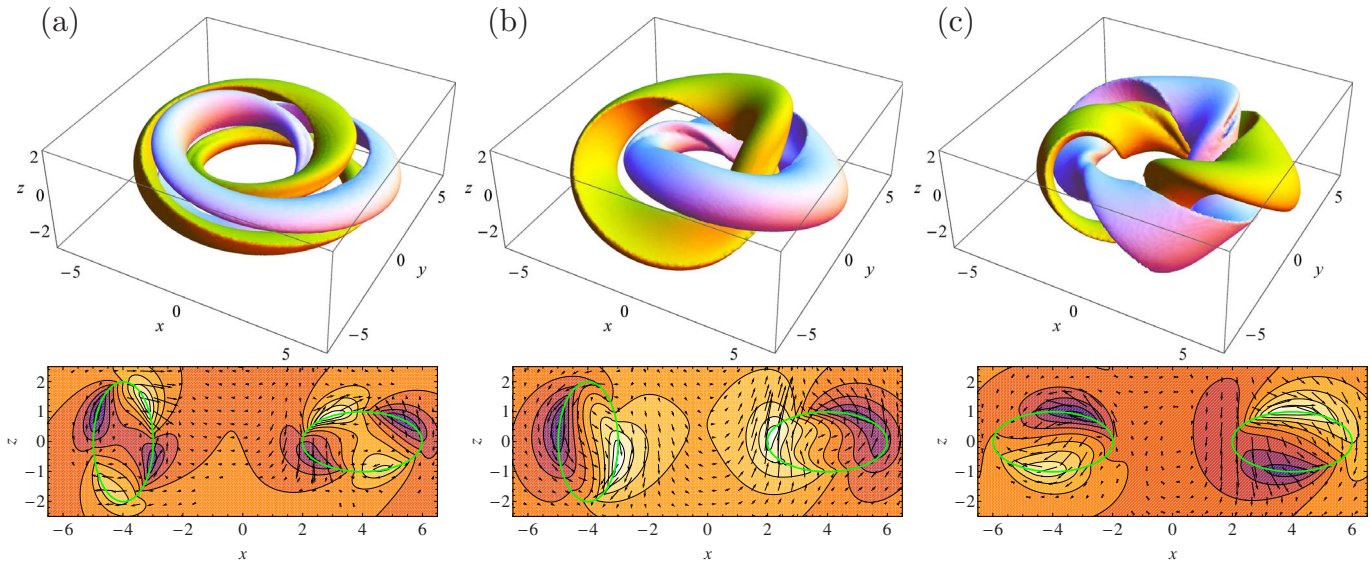

FIG. 3. (Color online) Upper panels: snapshots of the isosurfaces of B^2, where B is 1/3 of its maximum value, for a growing magnetic field generated by the Möbius flow in (a) run 1, (b) run 3, and (c) run 8 of Table I. Color indicates the general field direction along each isosurface (magnetic lines are not necessarily confined to the isosurfaces): red-blue (yellow-green) colors indicate magnetic field with $B_u>0$ ($B_u<0$) (cf. Fig. 1). Bottom panels show the respective cross sections $y=0$, with B_x and B_z shown with vectors and B_y, with color (shades of gray): positive (negative) values are represented by darker (lighter) shades.

TABLE I. Flow parameters and critical magnetic Reynolds number: the large radius of the channel R and the major semiaxis of its cross section a, with $b=1$ for the minor semiaxis, and $w=1$ at the channel surface; the number $2n$ of full twists of the cross section along the channel ($n=1/2$ is a Möbius strip), the v-symmetry number m (similar to the azimuthal wave number of cylindrical coordinates), the critical magnetic Reynolds number for the dynamo action, R_m^*, and the frequency of the marginal mode in the units of η/b^2. The last column illustrates the channel geometry showing its cross section at $u=0$, with the z axis on the left.

Run	R	a	n	N/m	R_m^*	ω	Cross-section at $u=0$
1	4	2	1/2	1/2	105	3.8	
2	4	2	1	1/1	25	1.4	
3	4	2	3/2	1/1	16	0.5	
8	4	2	2	2/1	19	1.8	
4	2	2	1/2	1/2	88	5.8	
11	2	2	3/2	1/1	17	0.5	
9	6	2	3/2	1/1	19	0.5	
5	4	4	1/2	1/2	55	1.8	
10	4	4	3/2	1/1	16	0.3	
6	2	1	3/2	1/1	20	1.1	
7	4	1	3/2	1/1	24	0.9	

in a box with periodic boundary conditions, with various numerical resolutions up to $240\times240\times180$ in x,y,z, respectively. The size of the box is sufficiently large to avoid excessive effect of the boundary conditions on the solution; most runs have a gap of a minimum size $2a$ between the channel and the box boundary. In all the simulations reported here, magnetic field at the boundary is at least two orders of magnitude weaker than in the dynamo region. Tests with a bigger computational box, where the minimum distance from the channel to the boundary is $4a$, confirm that its boundary has negligible effect on the solution (R_m^* changes by about 5–10 %). The value of R_m^* for the Ponomarenko dynamo is reproduced in the case $a=b$ and $R=10$ with accuracy 3% (in this limiting case, n controls the pitch of the streamlines).

Our simulations confirm that the Möbius flow is a dynamo. Since velocity shear is usually maximum at the surface of the channel, magnetic field strength is maximum there. The isosurfaces of B^2 represent two linked helical tubes shown in Fig. 3. This is not dissimilar to the magnetic field produced by the Ponomarenko dynamo, where the dominant mode has the azimuthal wave number $m=1$ (we note the obvious difference that the Ponomarenko dynamo was originally suggested for an infinite cylindrical region rather than a closed region discussed here). However, the leading dynamo mode in the Möbius flow with $n=1/2$ has a symmetry corresponding to $m=2$, i.e., each cross section $u=$const has four extrema of magnetic field (two pairs of opposite y directions) as shown in Fig. 3(a).

The symmetry selection of the dominant mode can be clarified using an analogy with the Ponomarenko dynamo. For this purpose we introduce a local cylindrical frame (ρ,Φ,Z) with the Z axis parallel to the channel axis ($w=0$); these variables correspond to the curvilinear coordinates in the Möbius channel as $\rho\to aw$, $\Phi\to v$, $Z\to Ru$. In the kinematic Ponomarenko dynamo with $\mathbf{V}=(0,\rho\Omega,V)$, the most easily excited magnetic mode $\mathbf{B}\propto\exp i(m\Phi+kZ)$ has $m/k\approx-V/\Omega$. By analogy, we expect that $m/k\approx-V_\phi/\Omega_\phi$ for the dynamo in the Möbius channel, where V_ϕ and Ω_ϕ are the components of the linear and angular velocities along the channel's longitudinal axis $w=0$, and m is the symmetry number with respect to the variable v (we note that the velocity field in the elliptical channel depends on v in the inertial frame, and magnetic field is not proportional to e^{imv}). If the channel cross section makes n complete turns as u changes by 2π (a Möbius strip has $n=1/2$), we have $2\pi n/\Omega_c=2\pi R/V_\phi$, and the period of the rotation of the channel cross section around the channel's longitudinal axis follows as $\Omega_c=nV_\phi/R$; we note that $V_\phi=$const across the channel cross section (see Fig. 2). Adopting Ω_c as a representative value of Ω, we obtain $m/k\approx-R/n$. The 2π-periodicity of $\mathbf{B}$ in u implies $k=-N/R$, where N is integer. Hence

$$N=[mn], \tag{7}$$

where square brackets denote the integer part. For a Möbius channel ($n=1/2$), we obtain $m=2$ and $N=1$ in accordance with the numerical results. We see from Table I that Eq. (7) holds for all models presented there as well as for several models with larger values of n which we explored. The channel of Fig. 3(a) has a half-rotation twist, $n=1/2$; therefore, magnetic lines can close on themselves only after two full rotations, i.e., $\mathbf{B}$ has the periodicity 4π in u and, correspondingly, the symmetry $m=2$. As follows from Eq. (7), $m=1$ for $N=1$ if $n=3/2$. This mode, shown in Fig. 3(b), is remarkable in that magnetic lines and the isosurfaces of B^2 twist by 2π radians along the channel whereas the channel itself twists by 3π. This means that magnetic lines shift along the v direction as u increases. In the mode shown in Fig. 3(c), the twists of the channel and magnetic field are both equal to 4π.

We have considered a selection of flow geometries presented in Table I. Runs 1–3 and 8 have the same channel geometry except for the number of full twists n: channels that envelop a Möbius strip (runs 1, 4, and also 5) generate the $m=2$ mode as discussed above, whereas channels with $n=1$ (run 2) and $n=3/2$ (runs 3, 6, 7, 9, 10, and 11) have $m=1$. The smallest R_m^* of about 16 is achieved in runs 3, 10, and 11, apparently because the ratio $V_\parallel/\Omega$ is closer to an optimum in these flows. Run 4 has a channel similar to that of run 1, but with smaller radius R; this facilitates the dynamo action, producing $R_m^*\approx88$, smaller than in run 1. A broader channel that touches the z axis, as in runs 5 and 10, is a still better dynamo. A channel with smaller R/a has smaller R_m^* apparently because of the stronger velocity shear

near the axis, where channel sections with oppositely directed velocities are the closest to each other.

A comparison with a toroidal dynamo whose parameters are similar to those of run 3 is provided with runs 6 and 7, where R_{m}^{*} is larger than that in run 3 by 25–50 %. As with an elliptical cross section, larger R/a, as in run 7, apparently hinders the dynamo. The channel with elliptical cross section in runs 3 and 9 has a smaller R_{m}^{*}, apparently because it extends to smaller distances from the rotation axis. The other relevant difference is that the cross section area of the channel is larger in runs 3 and 9, so the effective magnetic Reynolds number can be larger in those flows (see below). Flows with $n=3/2$ provide even lower values of R_{m}^{*} than the Ponomarenko dynamo (we note, however, that here R_{m} is based on the *smallest* dimension of the channel).

Similarly to the Ponomarenko dynamo, the oscillatory magnetic fields are produced, i.e., dynamo waves traveling in the u and v directions. The isosurfaces of B^2 are twisted in the same sense as the flow (Fig. 3), and magnetic lines are twisted similarly to the streamlines, so the current helicity $\mathbf{B}\cdot\boldsymbol{\nabla}\times\mathbf{B}$ has the same sign as the flow helicity $\mathbf{V}\cdot\boldsymbol{\nabla}\times\mathbf{V}$, where the magnetic field is strong. The frequencies of the marginal modes in the inertial frame are given in Table I (in units of η/b^2). For comparison, the frequency of the marginal mode of the most easily excited Ponomarenko dynamo is $\omega\approx 0.41$ in the same units. We note that the frequency of modes with the smallest R_{m}^{*} is close to this value.

The dynamo suggested here has several attractive features from the viewpoint of its laboratory implementation. An suitable apparatus for such an experiment could be a rotating toroidal shell filled with liquid sodium, as in the Perm dynamo experiment [4,7], which is braked to produce an inertial flow of sodium relative to the channel shell. A toroidal channel needs diverters to make the flow swirling. A Möbius flow can be produced using an insert of the corresponding shape (e.g., as in Fig. 1) fitted within the toroidal shell. To compare flows in channels with circular and elliptical cross sections, we renormalize R_{m} in the latter case by multiplying it by $a/b=2$. Thus, effectively, $R_{\mathrm{m}}^{*}=32$ for run 3, which is larger than $R_{\mathrm{m}}^{*}=20$ in the corresponding run 6 (dynamo in a torus).

However, it is more difficult to support a swirling flow in the torus. The localized divertors in the Perm experiment produce a rather inhomogeneous swirling flow, after the braking the average Ω grows slower than V_{ϕ}, and the swirling velocity peaks at a smaller value than V_{ϕ}. In a Möbius flow, the whole channel acts as a diverter. The swirling flow is established uniformly along the whole channel and will decay slower because the flow is not impeded by the diverters. Thus, a Möbius flow is likely to become supercritical earlier, and remain so for longer, than a comparable flow in a toroidal channel with diverters. Furthermore, this design could provide an opportunity to optimize the time variation of the flow by applying gradual (rather than abrupt, as in the Perm dynamo case) braking. Then the flow velocity relative to the shell can be kept at a level required to prolong the dynamo action further and, hence, to maximize the amplification factor of magnetic field. It is also possible that the elliptical shape of the channel cross section will prevent the development of turbulence.

We are grateful to J.-F. Pinton and A. Schekochihin for stimulating discussions. This work was supported by the Leverhulme Trust Grant No. F/00125/N, the Royal Society, RFBR-Ural Grant No. 06-01-00234, and the Russian Federation President Grant No. MK-4338.2007.1.

[1] P. Cardin and D. Brito, in *Mathematical Aspects of Natural Dynamos*, edited by E. Dormy and A. M. Soward (CRC Press, Boca Raton, 2007), pp. 361–407.

[2] Y. B. Ponomarenko, J. Appl. Mech. Tech. Phys. **14**, 775 (1973).

[3] A. Gailitis *et al.*, Phys. Rev. Lett. **84**, 4365 (2000).

[4] P. Frick, V. Noskov, S. Denisov, S. Kripchenko, D. Sokoloff, R. Stepanov, and A. Sukhanovsky, Magnetohydrodynamics **38**, 143 (2002).

[5] B. O. Koopman, Ann. Math. **27**, 424 (1926).

[6] L. Zabielski and A. J. Mestel, J. Fluid Mech. **573**, 237 (2007).

[7] W. Dobler, P. Frick, and R. Stepanov, J. Fluid Mech. **67**, 056309 (2003).

[8] A. D. Gilbert, Geophys. Astrophys. Fluid Dyn. **44**, 214 (1988).